Separation and Purification Technology 331 (2024) 125647

Contents lists available at ScienceDirect

Separation and Purification Technology

journal homepage: www.elsevier.com/locate/seppur

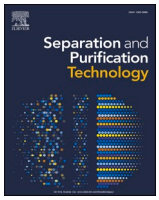

Silver nanoparticles catalyzed electrochemical hydrodechlorination of dichloromethane to methane in N,N-Dimethylformamide using water as hydrogen donor

Huan Wu [b,1], Liqing Chen [a,c,1], Can Tang [b], Xueyi Fan [a], Qi Liu [a,*], Yinghua Xu [b,*]

[a] School of Engineering, Hangzhou Normal University, Hangzhou 310036, PR China
[b] Petroleum and Chemical Industry Key Laboratory of Organic Electrochemical Synthesis, College of Chemical Engineering, Zhejiang University of Technology, Hangzhou 310014, PR China
[c] Baoding Qian Core Integrated Circuit (Hangzhou) Co., Ltd, Hangzhou 310020, PR China

ARTICLE INFO

Keywords
Chlorinated volatile organic compounds
Dichloromethane
Dechlorination
Silver
Nano effect

ABSTRACT

Silver nanoparticles (Ag NPs) were modified on Ag electrode in situ using the electrochemical redox method. The electrochemical hydrodechlorination (EHDC) performance of Ag NPs in N,N-Dimethylformamide (DMF) for a representative chlorinated volatile organic compound, dichloromethane (DCM), was studied. The results revealed that a large number of Ag NPs (~7 nm) were successfully deposited on the surface of Ag electrode. Be benefit to Nano effect, Ag NPs exhibited higher EHDC catalytic activity than bulk Ag and inhibited H_2 evolution. Under the catalysis of Ag NPs, the dechlorination of two Cl atoms on DCM was changed from synchronous dechlorination to asynchronous dechlorination. The EHDC efficiency of DCM in the three DMFs ranked from high to low as follows: weakly alkaline > Neutral > Weakly acidic. DCM at concentrations of 10–150 mM can be hydrodechlorinated to methane with ≥90% yield and ≥35% current efficiency.

1. Introduction

Chlorinated volatile organic compounds (Cl-VOCs), including chloromethanes, chloroethanes, and chloroethylenes, are widely used as solvents, degreasing agents and the production of commercial products [1–3]. Most Cl-VOCs are difficult to degrade naturally, and they have mutagenic, carcinogenic, and teratogenic effects on human health. In addition, the emission of Cl-VOCs into the atmosphere will delays the self-repairing of the ozone layer [4–6]. Therefore, the Ministry of Environmental Protection of China, the Environmental Protection Agency of the United States, and the European Commission have listed Cl-VOCs as a priority pollutant to control [1]. Cl atoms on Cl-VOCs are mainly responsible for the toxicity on human and ecological environment and it also contribute to the difficulty of degradation. If Cl atoms can be selectively removed from Cl-VOCs, the Cl-free product can be recycled as raw materials and fuel, or it can be emitted when it is safe to nature. Therefore, develop a series of efficient and environmentally friendly selective dechlorination technologies is highly desired for environmental protection [1,2].

The selective dechlorination methods of Cl-VOCs mainly include zero-valence metal reduction [7,8], catalytic hydrodechlorination of noble metals [9,10], biological dechlorination [11,12], and electrochemical hydrogenation dechlorination (EHDC) [13,14]. Compared with the mentioned dechlorination methods, EHDC has been widely studied by environmental scientists owing to the advantages of using water as hydrogen donor, no chemical reducing agent, normal operating temperature and pressure, and complete dechlorination [13–37]. Normally, EHDC in the aqueous phase is mainly used for the direct treatment of gas [13–15] or low-concentration Cl-VOCs [16–18]. However, EHDC in organic solvents can be carried out under a high concentration of reactants, which has more efficiency than EHDC in the aqueous phase used for direct treatment of low-concentration Cl-VOCs. It can be used to indirectly treat low-concentration Cl-VOCs in waste gas or wastewater (once they are extracted from water either through adsorption on activated carbon or organic solvent by air-stripping) [19,20]. It also can be used to destroy existing stocks of banned Cl-VOCs or those that are produced as byproducts in some industrial processes. Therefore, EHDC in organic solvents has a broad application prospect in treating Cl-VOCs.

* Corresponding authors.
E-mail addresses: qiliu@hznu.edu.cn (Q. Liu), xuyh@zjut.edu.cn (Y. Xu).
[1] These authors contributed equally to this work.

https://doi.org/10.1016/j.seppur.2023.125647
Received 25 September 2023; Received in revised form 25 October 2023; Accepted 6 November 2023
Available online 7 November 2023

$$R\text{-}Cl + e^- \leftrightarrow RCl^{\bullet -} \quad (1)$$

$$RCl^{\bullet -} \rightarrow R^{\bullet} + Cl^- \quad (2)$$

$$R\text{-}Cl + e^- \rightarrow R^{\bullet} + Cl^- \quad (3)$$

$$R^{\bullet} + e^- \leftrightarrow R^- \quad (4)$$

$$R^- + HA\ (\text{or } H^+) \rightarrow RH + A^- \quad (5)$$

$$R^{\bullet} + e^- + HA\ (\text{or } H^+) \leftrightarrow RH + A^- \quad (6)$$

$$AH + 2\ e^- \rightarrow H_2 + 2\ A^- \quad (7)$$

In organic solvents, the direct EHDC process of chlorinated organic compounds (R-Cl) can be basically described by Equations (1)–(6) [21–25]. The first electron transfer step and the C-Cl bond-breaking step occur successively (Eq. (1) + Eq. (2)) or simultaneously (Eq. (3)). Then, the free radical ($R^{\bullet}$) gains another electron and becomes the negative ionic free radical (R^-) (Eq. (4)). Finally, R^- combines with the proton to complete the EHDC (Eq. (5)), or $R^{\bullet}$ gains both an electron and a proton at the same time to complete the EHDC (Eq. (6)) [24,25]. For most Cl-VOCs, the first electron transfer step simultaneously occurs with the C-Cl bond-breaking step in the process (Eq. (3)). The cathode potential of the first electron transfer step is much higher than that of the second electron transfer step.

According to the reaction process, sufficient proton donors (such as water and acid) must be present in the electrolyte to achieve highly selective EHDC of Cl-VOCs. Especially, when the proton donor concentration is relatively low, Cl-VOCs will produce a polymerized coating on the electrode surface rather than be hydrogenated by proton, which greatly reduces the efficiency of EHDC [26,27]. For example, Hori et al. showed that the conversion of chloroform to methane was accomplished more efficiently on various metal electrodes when the water content was 1 M [26]. Rondinini et al. found that chloroform was reduced to methane at positive potential when the water/acetonitrile ratio was 1:1 [27]. Gennaro et al. developed an EHDC system using acetic acid as a proton donor that could achieve efficient dechlorination of all chloromethane in constant potential electrolysis [28]. Therefore, controlling the type and concentration of proton donors is one of the strategies to improve the EHDC efficiency of Cl-VOCs in organic solvents [26–29]. However, the overmuch proton donor will be reduced to H_2 (Eq. (7)), reducing the current efficiency of the EHDC. It is also important to design an electrode material that has ability in inhibiting the H_2 evolution.

In addition to the strategies mentioned above, electrode material with high catalytic activity for EHDC is also crucial. Scientists have tested the dechlorination performance of a large number of electrode materials in an organic solvent, including graphite [28], Fe [26,33], Zn [26,33], Au [26,33], Ag [19,26–33], Cu [20,32–34], Ni [26,32,33], Pb [26,31,33], Cd [26], Sn [26], Ti [26], Pt [26,32,33], Pd [33], and Ag alloy [27]. The results show that Ag, Pd, Au, and Cu exhibited much higher dechlorination activity than glass carbon (GC), and Ag has the best dechlorination property in organic solvents. To further improve the dechlorination activity of the catalytic material, Gennaro et al. also prepared Ag [35,36], Cu [36,37], and Pd [37,38] nanoparticles as catalytic materials for EHDC. However, due to these nanoparticles were much large and exhibited almost the same dechlorination intrinsic activity than that of their bulk materials, the Nano effect of the metal electrode on the EHDC in organic solvents have not been determined at present. Based on the Nano effect of the metal electrode on the EHDC in aqueous solution, which has been confirmed by Geneste [39], Brzózkat [17], Brudzisz [16] and our previous work [40–42], we suspected that the Nano effect of Ag was also exists in organic solvents. The intrinsic property of Ag in organic solvents was expected to be greatly improved by Nano effect.

In this work, an Ag nanoparticles modified Ag electrode (Ag NPs/Ag) was prepared to achieve more efficient EHDC and to confirm the Nano effect of Ag NPs at the same time. An EHDC system in organic solvents with Ag NPs/Ag, water, LiOH, and DMF as a cathode, proton donors, a pH controller, and a cathode solvent, respectively, was constructed. The system is expected to be paired with a possible anodic solution and anodic reaction in industrial applications.

2. Experiment

2.1. Preparation

Ag NPs/Ag electrode was prepared from bulk Ag electrode via electrochemical redox method. First, an Ag mesh (20 mm × 30 mm × 1 mm) was subjected to ultrasonication in acetone for 10 min to ensure complete de-oiling. Then, the ultrasonicated Ag mesh was treated with HCl aqueous solution (10%) for 10 min to remove oxides on its surface and washed with copious amounts of deionized water to prepare a bulk Ag electrode. Subsequently, cyclic voltammetry (CV) was performed using bulk Ag as working electrode to prepare Ag NPs/Ag. The Pt plate and Ag/AgCl electrode were used as the counter and reference electrodes, respectively. The CV was conducted in a 0.5 M NaCl aqueous solution, in the potential range of −0.6 V to 0.6 V, at scanning rate of 10 mV/s for four cycles.

Surface morphology of the prepared Ag electrodes was characterized using a scanning electron microscope (SEM, Carl Zeiss, Germany). The morphology of the Ag NPs was characterized using transmission electron microscopy (TEM, 300 kV, Tecnai G2 F30S-Twin microscope) and X-ray diffraction (XRD, Thermo, 45 kV and 40 mA, Cu Kα).

2.2. Electrochemical characterization

CV was applied to investigate EHDC catalytic property of different electrodes in DMF solution. Three electrode system was adapted: Ag NPs/Ag, bulk Ag, and GC were used as working electrode, respectively. Ag/Ag^+ electrode filled with 0.1 M $AgNO_3$ solution (0.79 V vs. SHE) was used as reference electrode; Pt electrode was used as counter electrode. The experiment was conducted under an N_2 atmosphere at a sweep rate of 50 mV/s at 25 °C.

Underpotential deposition (UPD) Pb layers were first deposited at −0.4 V vs. Ag/AgCl at different durations in 0.5 M $NaClO_4$ + 5 mM $HClO_4$ + 0.5 mM $Pb(ClO_4)_2$ aqueous solution. Then, linear sweep voltammetry (LSV) for anodic removal of the UPD Pb layer were conducted in 0.5 M $NaClO_4$ + 5 mM $HClO_4$ aqueous solution at a scan rate of 5 mV/s and a temperature of 25 °C, under N_2 atmosphere.

2.3. Electrolysis and analysis of products

DCM dechlorination produces gas, such as methane, the experiment was conducted in a closed H-type cell separated by a Nafion-117 ion membrane. Pt electrode and the prepared Ag electrode were used as an anode and a cathode, respectively. Unless otherwise noted, 50 mL of DMF solution containing 200 mM H_2O + 100 mM tetrabutylammonium tetrafluoroborate ($(C_4H_9)_4NBF_4$) + 40 mM LiOH was used as the cathode electrolyte, and 50 mL of 0.5 M H_2SO_4 aqueous solution was used as the anode electrolyte.

Concentration analysis of reactants in the aqueous solution: 1 mL of catholyte and 4 mL of H_2O were added into a sample bottle. After the sample bottle was heated and shaken in incubator for 15 min, the analysis was then performed using Thermo Fisher Trace 1300 chromatography with HP-INNOWAX column (30 m × 320 μm × 0.25 μm). FID detector temperature = 250 °C; H_2 flow rate = 30 mL/min; shunt ratio = 15:1; inlet temperature = 250 °C; flow rate in column = 1.2 mL/min.

Concentration analysis of reactants in the gas: the cathode of the H-type cell was connected with an 800 mL airbag. The gas in the cell was driven into the airbag by N_2. The product in the gas was measured using Agilent 7890A chromatography with HP-INNOWAX column (30 m × 320 μm × 0.25 μm). FID detector temperature = 250 °C; H_2 flow rate =

25 mL/min; shunt ratio = 20:1; column temperature = 36 °C. Inlet temperature = 250 °C; flow rate in column = 0.5 mL/min; detector heating temperature = 250 °C.

3. Results and discussion

3.1. Structural characterization

Ag NPs/Ag was prepared using the electrochemical redox method. Fig. 1A and 1B show SEM images of the surface of Ag electrodes before (Fig. 1A) and after (Fig. 1B) redox. As shown, Ag NPs/Ag had a rich porous structure after redox treatment, and numerous particles with a diameter of 100–500 nm were uniformly distributed on the surface. These particles were connected to each other, and gaps of hundreds of nanometers were evenly distributed between the particles.

To further understand the internal structure and composition of these particles, the Ag NPs were ultrasonically cleaned from Ag NPs/Ag. The SEM image of the Ag NPs/Ag after ultrasonication (Figure S1) showed that Ag particles on the surface were successfully cleaned. By observing the TEM image of shed Ag particles (Fig. 1C) and their particle size distribution (Fig. 1D), the large particles on the surface of the Ag NPs/Ag were accumulated by Ag NPs with an average size of 7 nm. XRD pattern also showed that the half-peak width of the diffraction peak of Ag NPs was much wider than that of bulk Ag (Fig. 1E), indicating the crystallinity of Ag NPs was decreased compared to bulk Ag, and Ag NPs had more edge/corner Ag atoms than bulk Ag.

We have found that when Ag was oxidized to AgCl, the electrode surface was only roughened, but no obvious porous structure appeared (Figure S2). However, when AgCl was reduced to Ag, the porous structure appeared immediately. Therefore, the formation of these porous structures is caused by the de-intercalation of Cl^- during the process of Ag redox in NaCl solution. The repeatedly intercalation and de-intercalation of Cl^- of Ag not only constructed the porous structure, but also modified Ag NPs. In addition, the specific surface areas of Ag NPs/Ag and bulk Ag were also measured using anode stripping curves of UPD Pb. As shown in Fig. 1F and S3, the specific surface area of Ag NPs/Ag was 10.3 times that of bulk Ag. These results provided a good basis for us to study the Nano effect of Ag electrodes in EHDC of Cl-VOCs in organic solvents and Ag NPs/Ag have potential to achieve efficient EHDC on Ag NPs/Ag.

3.2. Intrinsic catalytic activity

We investigated the CV responses of GC (Fig. 2A), bulk Ag (Fig. 2B), and Ag NPs/Ag (Fig. 2C) electrodes to DCM in DMF solutions at different pH (≈ 5.5, 7, and 8.5) to compare their intrinsic EHDC catalytic activity. The reduction onset potential and reduction peak potential of DCM at the three electrodes in the three DMFs from positive to negative were Ag NPs/Ag > bulk Ag > GC. Among them, the reduction onset potential of DCM on Ag NPs/Ag in neutral and weakly alkaline DMFs positively shifted by approximately 400 mV compared with bulk Ag. The results showed that the EHDC catalytic activity of Ag NPs/Ag was much better than that of bulk Ag. This result is significantly different from the report of Gennaro et al. [35]. The underlying reason for the difference in the results might be because the size of Ag NPs on the prepared Ag NPs/Ag (7 nm) was much smaller than the size of Ag nanoparticles on their electrodes (192–394 nm). Generally, the surface of metal nanoparticle contains plane atoms and corner atoms. When the size of nanoparticles is several hundred nanometers, the proportion of corner atoms will be relatively small. In contrast, when the size of nanoparticles is a few nanometers, the proportion of corner atoms will significantly increase. Therefore, if the catalytic activity of corner Ag atoms is better than that of plane Ag atoms, small Ag nanoparticles will show higher activity. Mussini et al. have confirmed that Ag atoms on different crystal faces have various electrochemical debromination activities [43]. Their result confirmed that the above speculation is theoretically possible. However, there is no direct evidence to support this theory at present.

In addition, no significant difference was observed between the reduction onset potential and reduction peak current of DCM on CV curves of Ag NPs/Ag in DMFs at different pH (Fig. 2C). Therefore, the protonation step of the anion radical (Eq. (5)) or the step in which the radical simultaneously gained an electron and a proton (Eq. (6)) rapidly occurred and it was barely not affected by the concentration of H^+. Peaks corresponding to acetic acid or H^+ (dissociation from acetic acid) reduction reactions appeared within the potential range of DCM reduction in weakly acidic DMF solution, which might compete with dechlorination. Therefore, neutral and weakly alkaline DMFs may achieve higher DCM dechlorination efficiency than weakly acidic DMFs.

In addition, the reduction peak current of DCM on Ag NPs/Ag was almost same or slightly lower than that on bulk Ag, even though the specific surface area of Ag NPs/Ag was 10 times that of bulk Ag. A similar phenomenon was observed in our previous work [40]. The main

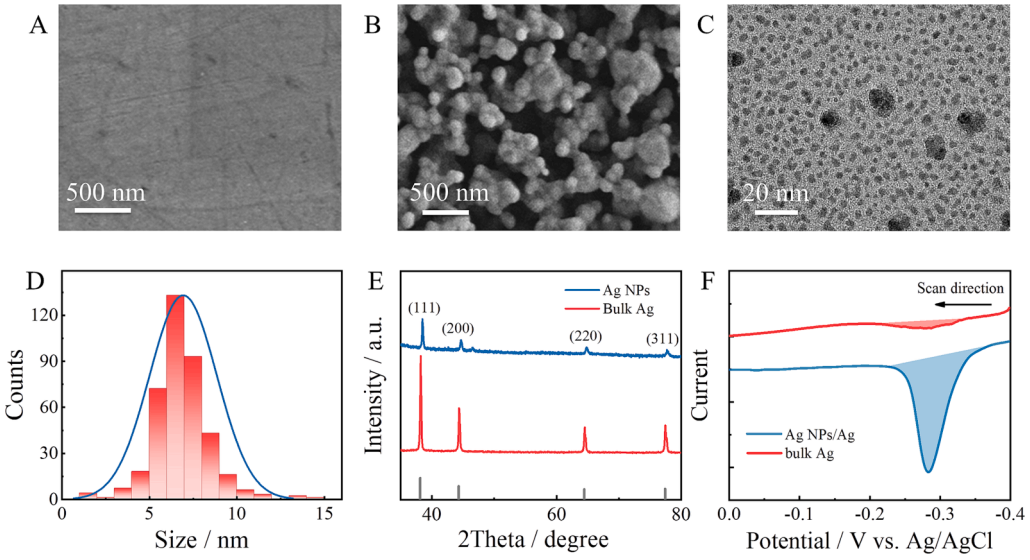

Fig. 1. Characterization of Bulk Ag and Ag nanoparticle modified Ag (Ag NPs/Ag) electrode. SEM images of (A) Bulk Ag and (B) Ag NPs/Ag. TEM image (C) and size distributions (D) of Ag NPs ultrasonically removed from Ag NPs/Ag electrode. (E) XRD of Bulk Ag and Ag NPs. (F) Linear sweep curves (LSVs) for anodic removal of UPD Pb layer deposited on prepared electrodes.

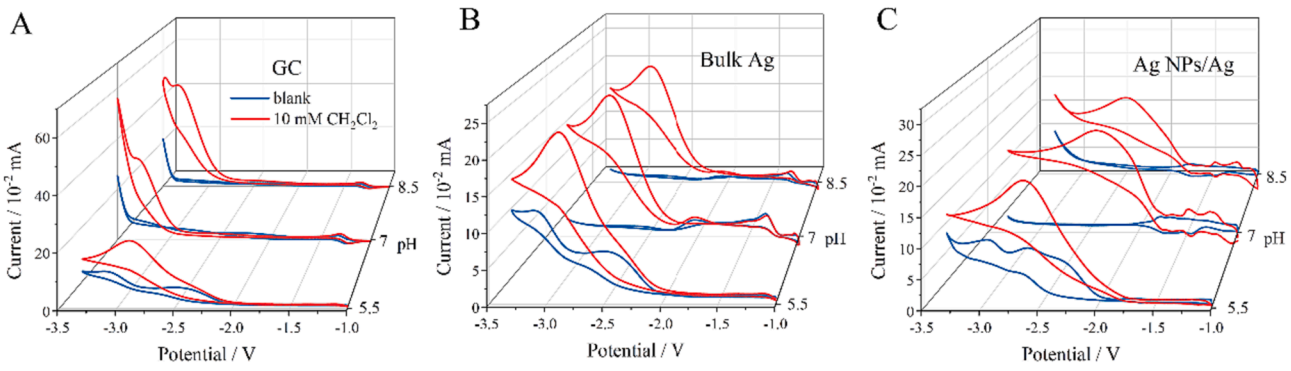

D

Reduction onset potential / V

Cathode	pH = 5.5	pH = 7	pH = 8.5
GC	-2.2	-2.9	-2.7
Bulk Ag	-2.0	-2.2	-2.2
Ag NPs/Ag	-1.75	-1.75	-1.8

E

Reduction peak current / 10^{-2} mA mm^{-2}

Cathode	pH = 5.5	pH = 7	pH = 8.5
GC	7.4	7.6	6.7
Bulk Ag	4.7	7.0	5.7
Ag NPs/Ag	6.4	6.5	5.4

Fig. 2. Cyclic voltammetry (CV) curves of 10 mM DCM recorded on (A) disk GC (Ø 3 mm), (B) Bulk Ag (Ø 2 mm) and (C) Ag NPs/Ag electrode (Ø 2 mm), in different solution (pH = 5.5 ↔ DMF + 100 mM $(C_4H_9)_4NBF_4$ + 200 mM H_2O + 40 mM CH_3COOH; pH = 7 ↔ DMF + 100 mM $(C_4H_9)_4NBF_4$ + 200 mM H_2O; pH = 8.5 ↔ DMF + 100 mM $(C_4H_9)_4NBF_4$ + 200 mM H_2O + 40 mM LiOH). (D) Reduction onset potential and (E) Peak current of EHDC corresponding to A, B and C.

reason was that the solution was stationary during the CV test; thus, the thickness of the diffusion layer of DCM was relatively larger than the pore size of the three-dimensional structure constructed by Ag particles on Ag NPs/Ag. Consequently, the area available for diffusion current was significantly reduced, and the reduction peak current of the reactant was only related to the projected area of the electrode instead of the real area of the electrode.

Stirring can reduce the diffusion layer thickness of the reactants on the electrode surface, so we further studied the LSV curves of DCM on two Ag electrodes at different stirring speeds (Figure S4). The result showed that the reduction current of DCM on Ag NPs/Ag was extremely close to that on bulk Ag electrodes without stirring and at a stirring speed of 70 rpm (compared at −3 V). When stirring speeds were increased to 100 and 130 rpm, the reduction current of DCM on Ag NPs/Ag was significantly higher than that on bulk Ag electrodes, indicating that the thickness of diffusion layer of DCM on Ag NPs/Ag surface was close to the size of Ag particles and the gap between particles on Ag NPs/Ag. These results show that rigorous stirring of the cathode solution during electrolysis can accelerate the EHDC of DCM on Ag NPs/Ag.

We recorded the reduction onset potential of DCM and MCM on Ag NPs/Ag, bulk Ag, and GC electrodes (Fig. 3). The reduction peak potential of DCM was lower than that of MCM, resulting in only one reduction peak for DCM on the CV curves (Fig. 3A, 3B and 3C). To compare the catalytic effect of Ag, ΔE_0^{cat} was described as positive movement of the reduction onset potential, which is based on the difference of reduction onset potential with GC (GC is basically has no catalytic property for EHDC). The ΔE_0^{cat} values of Ag NPs/Ag to DCM and MCM were + 1.1 V and + 1.2 V, respectively. The ΔE_0^{cat} values of bulk Ag to DCM and MCM were + 0.6 V and + 0.95 V, respectively. The greater value of ΔE_0^{cat} presents the barrier of activation energy is decreased more obviously by catalytic effect of Ag. It showed that the catalytic activity of Ag NPs/Ag was superior to that of bulk Ag for both DCM and MCM, and the catalytic effect of both Ag NPs/Ag and bulk Ag electrodes on MCM are stronger than those on DCM.

In addition, as shown in Fig. 3B and 3C, the reduction onset potential of DCM on Ag NPs/Ag (−1.7 V) was more positive than that of MCM (−1.95 V), while the reduction onset potential of DCM (−2.2 V) on bulk Ag electrode was almost the same as that of MCM (−2.2 V). For bulk Ag, the dechlorination potentials of DCM and MCM are similar, thus the two Cl atoms on DCM are dechlorinated synchronously. For Ag NPs/Ag, since the dechlorination potential of the two Cl atoms are different, in this case the two Cl atoms on DCM will dechlorinate asynchronously.

The difference in reduction onset potential of DCM and MCM caused by Nano effect of Ag NPs has a certain academic value. For most chlorinated organics, the reduction onset potential will be more positive with more Cl atoms on both the inert GC electrode [19,21,24,27,34] and the catalytic electrode [19,27,34] except bulk Ag [28] and bulk Cu [20]. Therefore, the phenomenon that "the reduction onset potential of DCM on Ag NPs/Ag is more positive than that of MCM" may provide important data for the analysis of this special case, which will help scientists deepen and improve the EHDC mechanism of Cl-VOCs on catalytic electrodes.

3.3. *Inhibiting the H_2 evolution*

In the large-scale application for EHDC of Cl-VOCs in organic solvents, the ideal anodic solution is aqueous solution. Thus, the water in the anodic solution will inevitably gradually penetrate through the ion membrane into the cathode organic solvent. Therefore, we further studied the effect of water content in DMF on the EHDC. As shown in Fig. 4, with the increasing water concentration, the reduction onset potential and reduction peak potential of DCM on bulk Ag electrode did not change. However, the H_2 evolution potential rapidly moved to positive (especially when water contents were 1 M and 2.5 M, the H_2 evolution onset potential were −2.85 V and −2.65 V, respectively). It indicates that the addition of water promoted the H_2 evolution on bulk Ag. As a competitive reaction, H_2 evolution can seriously hinder the progress of EHDC. On the contrary, with the water concentration increasing, the reduction onset potential of DCM on Ag NPs/Ag positively moved. More importantly, the H_2 evolution potential slowly moved to positive at this prosses. the H_2 evolution onset potential of Ag NPs/Ag were −3.1 V and −3.0 V, respectively, when water contents were 1 M and 2.5 M. It could be calculated that, compared to bulk Ag, the ability of inhibiting H_2 evolution of Ag NPs/Ag is about 350 mV at the water content of 2.5 M and is about 250 mV at the water content of 1 M. This results not only show that the increase in water further improved

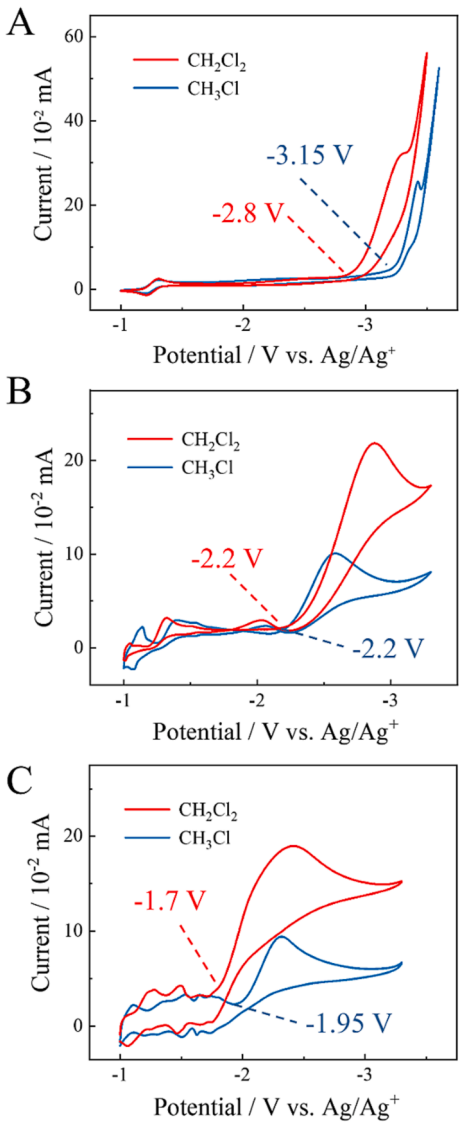

Fig. 3. Cyclic voltammetry (CV) curves of 10 mM DCM and MCM recorded on disk (A) GC (Ø 3 mm), (B) Bulk Ag (Ø 2 mm) and (C) Ag NPs/Ag electrode (Ø 2 mm) in DMF + $(C_4H_9)_4NBF_4$ + 200 mM H_2O. The dot line marked reduction onset potential of DCM and MCM dechlorination.

EHDC activity of Ag NPs/Ag, but also indicate that Ag NPs/Ag had better performance than bulk Ag electrodes in inhibiting the reduction of water to H_2. The property of Ag NPs/Ag in inhibiting H_2 evolution would be attributed to rich Ag micro-particles and Ag NPs.

Ag NPs/Ag had more adaptability for a wider range of water concentrations than bulk Ag electrodes. It is important for the EHDC of Cl-VOCs in organic solvents. The high current efficiency can be achieved even if there is a higher water content in the organic solvent of the cathode chamber. This feature of Ag NPs/Ag is important in engineering applications.

3.4. Electrolysis

As shown in Fig. 5A, we compared the EHDC performance of Ag NPs/Ag and bulk Ag electrodes on DCM using constant current electrolysis (using optimized current density, Figure S5). In the electrolysis process, H^+ in anodic solution entered cathodic solution continuously through the ionic membrane. As a result, the weakly alkaline cathodic solution was used for electrolysis to ensure that the cathodic solution did not transform into acid during whole electrolytic process. As shown in

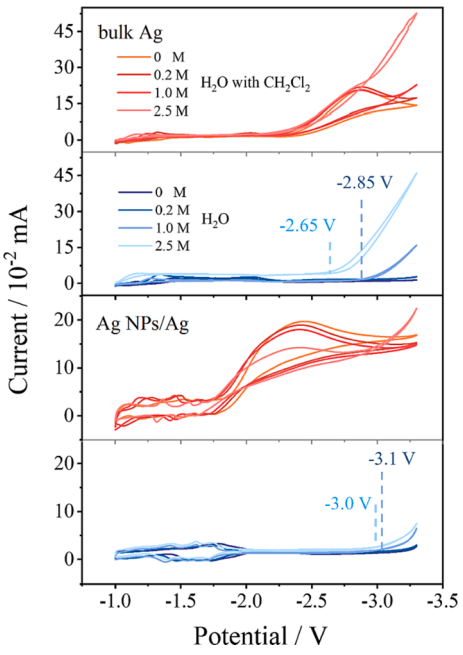

Fig. 4. Cyclic voltammetry (CV) curves of 10 mM DCM recorded on disk Bulk Ag (Ø 3 mm) and disk Ag NPs/Ag (Ø 2 mm) electrodes, in DMF + 0.1 M $(C_4H_9)_4NBF_4$ with different concentration of H_2O.

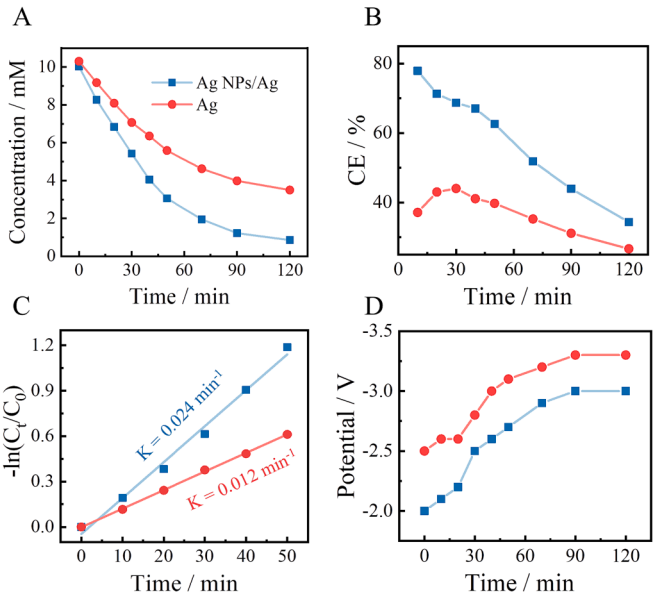

Fig. 5. Effect of cathode material (mesh Bulk Ag and Ag NPs/Ag with a project area of 2 × 3.5 cm^2) on the dechlorination of 10 mM DCM. (A) Concentration profiles of DCM, (B) apparent rate constant, K, (C) current efficiency and (D) electrode potential during the dechlorination. Catholyte = 50 mL DMF + $(C_4H_9)_4NBF_4$ + 200 mM H_2O + 40 mM LiOH under N_2 atmosphere, anolyte = 50 mL 0.5 M H_2SO_4 aqueous solution, temperature = 25 °C, applied current = 50 mA.

Fig. 5B, the conversion of DCM and dechlorination current efficiency of Ag NPs/Ag were significantly higher than that of bulk Ag during whole electrolytic process. When the electrolysis time was 120 min, the conversion of DCM on Ag NPs/Ag was 92%, while that of bulk Ag was 68%. First-order kinetic fitting of the EHDC of DCM (Fig. 5C) showed that the apparent rate constant of DCM on the Ag NPs/Ag was about twice that on the bulk Ag. In addition, Ag NPs/Ag electrode consistently maintained a more positive cathode potential than bulk Ag electrode

(Fig. 5D), which helps to reduce the cell voltage and prevent H_2 evolution. In practical industrial applications, the decrease of voltage is very important to save energy consumption. The dechlorination performance of the Ag NPs/Ag electrode for DCM owing to its higher catalytic activity, larger specific surface area, and better inhibitory effect on water reduction to H_2.

The effect of pH on electrolysis rate of DCM was investigated. As shown in Fig. 6A, the electrolysis rate of DCM on the Ag NPs/Ag electrode in the three different pH cathode solutions were ranked in the following order from high to low: weakly alkaline > neutral > weakly acidic. This result is consistent with the result of the CV experiment under different pH conditions. The EHDC rate in weakly acidic solution was the lowest due to its lower pH during the electrolysis process (Fig. 6B), lower pH leading to more severe H_2 evolution. Fig. 6C shows the material conversion in the DCM dechlorination process. The concentration of MCM was relatively low throughout the DCM dechlorination process (Fig. 6D), which probably because the potential of Ag NPs/Ag (Fig. 5D) was more negative than the reduction onset potential of MCM (Fig. 3C) during the electrolysis. During the electrolysis, most of MCM produced by DCM dechlorination was further dechlorinated to methane before it left the electrode surface. In addition, the total concentration added by DCM, MCM and methane was equal to the initial concentration of DCM. This result shows that the EHDC of DCM to methane is highly selective.

Finally, we verified feasibility of Ag NPs/Ag on various concentrations of DCM and stability of Ag NPs/Ag. Fig. 6D shows the conversion of DCM at different concentrations (10–150) mM by using Ag NPs/Ag, a conversion of DCM of more than 92% can be achieved on Ag NPs/Ag. In addition, the DCM dechlorination rate was approximately same in five consecutive electrolysis (Figure S6). These results show that the EHDC system developed in this work has a broad application prospect in practical engineering applications.

3.5. Mechanistic origin of catalytic activity

According to basic catalysis theory, the EHDC activity of Ag superior to GC is probably due to its adsorption of reactants, intermediates, and products. As shown in Fig. 7A, the adsorption effect of Ag significantly reduced the reaction energy barrier, which led to the reaction path changes from the blue trajectory to the red trajectory. The intrinsic catalytic activity of Ag NPs/Ag was better than that of bulk Ag (i.e., the dechlorination onset potential of Ag NPs/Ag was more positive). This phenomenon may also be attributed to the different adsorption properties caused by the different nanostructure of Ag particles on the surface. These adsorptions significantly affect thermodynamic and kinetic characteristics of dechlorination reactions.

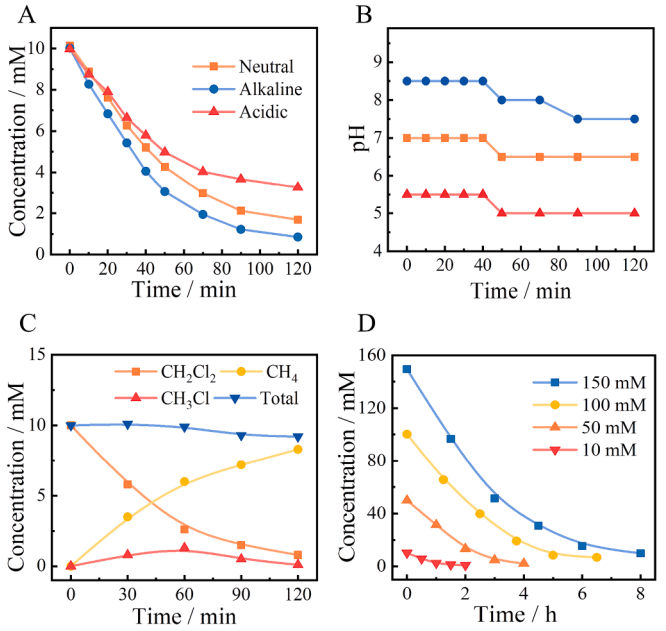

Fig. 6. Effect of (A and B) catholyte pH and (D) reactant initial concentration on the dechlorination of DCM; (C) product selectivity and carbon mass balance. Catholyte = 50 mL DMF + $(C_4H_9)_4NBF_4$ + 200 mM H_2O + X mM LiOH under N_2 atmosphere, anolyte = 50 mL 0.5 M H_2SO_4 aqueous solution, temperature = 25 °C, applied current = Y mA. When initial concentrations of DCM were 10, 50, 100, 150 mM, X = 40, 100, 250, 375 mM, Y = 50, 100, 150, 200 mA.

EHDC of DCM on the Ag electrode can be described as shown in Fig. 7B [22,23,28]. According to Gennaro et al. [22,23]. The first electron transfer step (Step. 2) of DCM dechlorination is significantly more thermodynamically difficult than the second electron transfer step (Step. 4). In other words, the equilibrium potential of the first electron transfer step is more positive than that of the second electron transfer step. Therefore, the dechlorination reaction can be accelerated by adjusting thermodynamic and kinetic characteristics of the first electron transfer step. Specifically, in thermodynamics, adsorption of the first electron transfer step product ($R^{\bullet}$ and Cl^-) on catalytic electrode can make its equilibrium potential move positively, which is conducive to dechlorination reaction. The stronger adsorption, the greater movement. In addition, in kinetics, adsorption of the transition-state intermediates ($[R\text{-}Cl_{ads}]^{\neq}$) of the first electron transfer step by catalytic electrode reduces the activation energy, thus accelerating the speed of the transfer step and the entire dechlorination reaction.

To investigate the conjecture in thermodynamics, the effect of Ag on the adsorption of $R^{\bullet}$ and Cl^- was studied. First, CV experiments of DCM were conducted under different Cl^- concentrations, and the results are shown in Figure S7. The reduction onset potential and reduction peak potential of DCM almost did not change, only the peak current moderately decreased with the increasing of Cl^-. The results showed that the adsorption between Cl^- and Ag NPs/Ag was relatively weak within the potential range of DCM reduction, and the catalytic activity of Ag NPs/Ag was not mainly due to its adsorption of Cl^-. In addition, if a pre-peak (caused by the peak positively shifted of the first electron transfer step) is not observed on the CV curve of MCM (Fig. 3B and 3C), the strong adsorption of $R^{\bullet}$ on Ag NPs/Ag can also be excluded [23]. Therefore, the thermodynamic characteristics of Ag NPs do not seem to be the main reason for the enhancement of their catalytic activity. Consequently, the EHDC activity of Ag NPs/Ag might be attributed to its kinetic characteristics (stronger adsorption of $[R\text{-}Cl_{ads}]^{\neq}$), which reduced the activation energy of the first electron transfer step and the overpotential.

4. Conclusions

Ag NPs (~7 nm) was modified on Ag electrode in-situ by electrochemical redox method. The prepared Ag NPs/Ag electrode exhibited higher catalytic dechlorination activity than bulk Ag and showed good ability to inhibits H_2 evolution. Compared to bulk Ag, the EHDC potential of DCM shifted positively by 400 mV on Ag NPs and the dechlorination of two Cl atoms on DCM changed from synchronous dechlorination to asynchronous dechlorination. DCM with various concentrations (10–150 mM) was dechlorinated to methane with yield of ≥90%. The property of Ag NPs/Ag electrode originated from the characteristics of Ag and the Nano effect of Ag NPs, which changed the kinetics of EHDC.

CRediT authorship contribution statement

Huan Wu: Methodology, Investigation, Writing - original draft. **Liqing Chen:** Investigation, Visualization. **Can Tang:** Validation, Visualization. **Xueyi Fan:** Investigation. **Qi Liu:** Conceptualization, Funding acquisition, Resources. **Yinghua Xu:** Conceptualization, Project administration, Funding acquisition, Resources, Writing - review & editing.

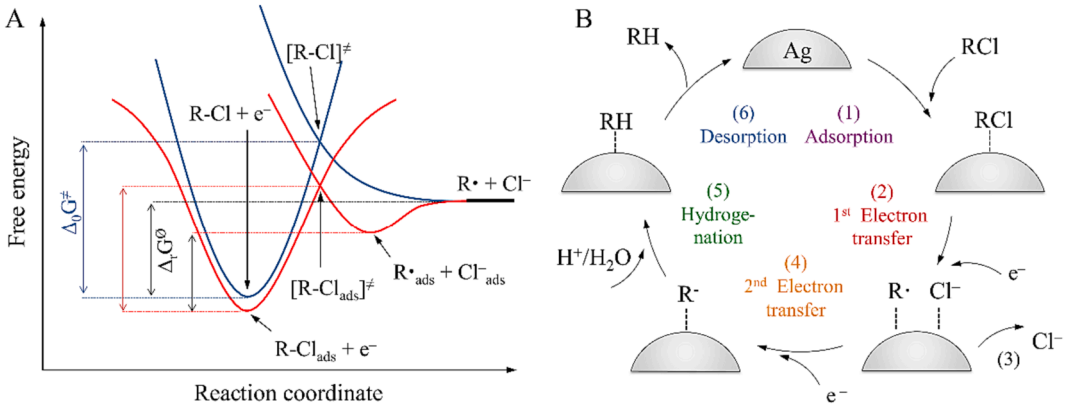

Fig. 7. (A) Energy barrier changing of EHDC under catalytic effect and (B) EHDC path of Cl-VOCs catalyzed by Ag.

Declaration of Competing Interest

The authors declare that they have no known competing financial interests or personal relationships that could have appeared to influence the work reported in this paper.

Data availability

Data will be made available on request.

Acknowledgements

This research was supported by the funds from the National Natural Science Foundation of China [21576238], Zhejiang Provincial Key Research and Development Program [2020C03085], Development of Industrial Technology for the Preparation of Chloroaminopyridine Acid by Bipolar Membrane Electrolysis [KYY-HX-20210385], and Hangzhou Science and Technology Development Foundation of China [20190101A02].

Appendix A. Supplementary data

Supplementary data to this article can be found online at https://doi.org/10.1016/j.seppur.2023.125647.

References

[1] B. Huang, C. Lei, C. Wei, G. Zeng, Chlorinated volatile organic compounds (Cl-VOCs) in environment — sources, potential human health impacts, and current remediation technologies, Environ. Int. 71 (2014) 118–138, https://doi.org/10.1016/j.envint.2014.06.013.

[2] C. Dai, Y. Zhou, H. Peng, S. Huang, P. Qin, J. Zhang, Y. Yang, L. Luo, X. Zhang, Current progress in remediation of chlorinated volatile organic compounds: A review, J. Ind. Eng. Chem. 62 (2018) 106–119, https://doi.org/10.1016/j.jiec.2017.12.049.

[3] W. Tsai, Fate of Chloromethanes in the Atmospheric Environment: Implications for Human Health, Ozone Formation and Depletion, and Global Warming Impacts, Toxics 5 (2017), https://doi.org/10.3390/toxics5040023.

[4] D.E. Oram, M.J. Ashfold, J.C. Laube, L.J. Gooch, S. Humphrey, W.T. Sturges, E. Leedham-Elvidge, G.L. Forster, N.R.P. Harris, M.I. Mead, A.A. Samah, S. M. Phang, C.-F. Ou-Yang, N.-H. Lin, J.-L. Wang, A.K. Baker, C.A.M. Brenninkmeijer, D. Sherry, A growing threat to the ozone layer from short-lived anthropogenic chlorocarbons, Atmos. Chem. Phys. 17 (2017) 11929–11941, https://doi.org/10.5194/acp-17-11929-2017.

[5] R. Hossaini, M.P. Chipperfield, S.A. Montzka, A.A. Leeson, S.S. Dhomse, J.A. Pyle, The increasing threat to stratospheric ozone from dichloromethane, Nat. Commun. 8 (2017) 15962, https://doi.org/10.1038/ncomms15962.

[6] M. An, L.M. Western, D. Say, L. Chen, T. Claxton, A.L. Ganesan, R. Hossaini, P. B. Krummel, A.J. Manning, J. Mühle, S. O'Doherty, R.G. Prinn, R.F. Weiss, D. Young, J. Hu, B. Yao, M. Rigby, Rapid increase in dichloromethane emissions from China inferred through atmospheric observations, Nat. Commun. 12 (2021) 7279, https://doi.org/10.1038/s41467-021-27592-y.

[7] M. Leah, T. Paul, Reductive Dehalogenation of Chlorinated Methanes by Iron Metal, Environ. Sel. Technol. 28 (1994) 2045–2053, https://doi.org/10.1021/es00061a012.

[8] T.N. Boronina, K.J. Klabunde, G.B. Sergeev, Dechlorination of carbon tetrachloride in water on an activated zinc surface, Mendeleev Commun. 8 (1998) 154–155, https://doi.org/10.1070/MC1998v008n04ABEH000952.

[9] K. Mackenzie, H. Frenzel, F.-D. Kopinke, Hydrodehalogenation of halogenated hydrocarbons in water with Pd catalysts: Reaction rates and surface competition, Appl. Catal. B Environ. 63 (2006) 161–167, https://doi.org/10.1016/j.apcatb.2005.10.004.

[10] C. Hyun, H. Sun, S. Jae, H. Kyung, G. Young, Effects of Pt Precursors on Hydrodechlorination of Carbon Tetrachloride over Pt/Al2O3, J. Catal. 166 (1997) 284–293, https://doi.org/10.1006/jcat.1997.1508.

[11] Y. Lai, A. Ontiveros-Valencia, T. Coskun, C. Zhou, B.E. Rittmann, Electron-acceptor loadings affect chloroform dechlorination in a hydrogen-based membrane biofilm reactor, Biotechnol. Bioeng. 116 (2019) 1439–1448, https://doi.org/10.1002/bit.26945.

[12] D. Rodríguez-Fernández, C. Torrentó, M. Guivernau, M. Viñas, D. Hunkeler, A. Soler, C. Domènech, M. Rosell, Vitamin B12 effects on chlorinated methanes-degrading microcosms: Dual isotope and metabolically active microbial populations assessment, Sci. Total Environ. 621 (2018) 1615–1625, https://doi.org/10.1016/j.scitotenv.2017.10.067.

[13] O. Lugaresi, H. Encontre, C. Locatelli, A. Minguzzi, A. Vertova, S. Rondinini, C. Comninellis, Gas-phase volatile organic chloride electroreduction: A versatile experimental setup for electrolytic dechlorination and voltammetric analysis, Electrochem. Commun. 44 (2014) 63–65, https://doi.org/10.1016/j.elecom.2014.04.017.

[14] S. Rondinini, G. Aricci, Ž. Krpetić, C. Locatelli, A. Minguzzi, F. Porta, A. Vertova, Electroreductions on Silver-Based Electrocatalysts: The Use of Ag Nanoparticles for CHCl3 to CH4 Conversion, Fuel Cells 9 (2009) 253–263, https://doi.org/10.1002/fuce.200800083.

[15] C. Williams, G. McCarver, A. Lashgari, K. Vogiatzis, J. Jiang, Electrocatalytic Dechlorination of Dichloromethane in Water Using a Heterogenized Molecular Copper Complex, Inorg. Chem. 60 (2021) 4915–4923, https://doi.org/10.1021/acs.inorgchem.0c03833.

[16] A. Brudzisz, G.D. Sulka, A. Brzózka, A facile approach to silver nanowire array electrode preparation and its application for chloroform reduction, Electrochim. Acta 362 (2020), https://doi.org/10.1016/j.electacta.2020.137110.

[17] A. Brzózka, A. Jeleń, A.M. Brudzisz, M.M. Marzec, G.D. Sulka, Electrocatalytic reduction of chloroform at nanostructured silver electrodes, Electrochim. Acta 225 (2017) 574–583, https://doi.org/10.1016/j.electacta.2016.12.111.

[18] M. Wu, J. Hu, Y. Wu, Y. Tang, Y. Zhang, Y. Guan, Z. Lou, Z. Yu, J. Yu, Enhanced dechlorination of an enzyme-catalyzed electrolysis system by ionic liquids: Electron transfer, enzyme activity and dichloromethane diffusion, Chemosphere 281 (2021), 130913, https://doi.org/10.1016/j.chemosphere.2021.130913.

[19] C. Durante, A.A. Isse, A. Gennaro, Electrocatalytic dechlorination of polychloroethylenes at silver cathode, J. Appl. Electrochem. 43 (2012) 227–235, https://doi.org/10.1007/s10800-012-0483-4.

[20] A.A. Isse, B. Huang, C. Durante, A. Gennaro, Electrocatalytic dechlorination of volatile organic compounds at a copper cathode. Part I: Polychloromethanes, Appl. Catal. B Environ. 126 (2012) 347–354, https://doi.org/10.1016/j.apcatb.2012.07.004.

[21] H. Tang, Z. Bian, Y. Peng, S. Li, H. Wang, Stepwise dechlorination of chlorinated alkenes on an Fe-Ni/rGO/Ni foam cathode: Product control by one-electron-transfer reactions, J. Hazard. Mater. 433 (2022), 128744, https://doi.org/10.1016/j.jhazmat.2022.128744.

[22] A.A. Isse, L. Falciola, P.R. Mussini, A. Gennaro, Relevance of electron transfer mechanism in electrocatalysis: the reduction of organic halides at silver electrodes, Chem. Commun. (2006) 344–346, https://doi.org/10.1039/b513801a.

[23] A.A. Isse, S. Gottardello, C. Durante, A. Gennaro, Dissociative electron transfer to organic chlorides: Electrocatalysis at metal cathodes, Phys. Chem. Chem. Phys. 10 (2008) 2409–2416, https://doi.org/10.1039/b719936h.

[24] B. Huang, J. Long, W. Chen, Y. Zhu, G. Zeng, C. Lei, Linear free energy relationships of electrochemical and thermodynamic parameters for the electrochemical reductive dechlorination of chlorinated volatile organic

compounds (Cl-VOCs), Electrochim. Acta 208 (2016) 195–201, https://doi.org/10.1016/j.electacta.2016.04.182.
[25] A.A. Isse, A. De Giusti, A. Gennaro, One- versus two-electron reaction pathways in the electrocatalytic reduction of benzyl bromide at silver cathodes, Tetrahedron Lett. 47 (2006) 7735–7739, https://doi.org/10.1016/j.tetlet.2006.08.123.
[26] B. Arkadiusz, M. Wieslaw, Technological aspects of the synthesis of 2,4-dichlorophenol, Pol. J. Chem. Technol. 11 (2009) 21–30, https://doi.org/10.2478/v10026-009-0019-9.
[27] S. Rondinini, A. Vertova, Electrocatalysis on silver and silver alloys for dichloromethane and trichloromethane dehalogenation, Electrochim. Acta 49 (2004) 4035–4046, https://doi.org/10.1016/j.electacta.2003.12.061.
[28] C. Durante, A.A. Isse, G. Sandonà, A. Gennaro, Electrochemical hydrodehalogenation of polychloromethanes at silver and carbon electrodes, Appl. Catal. B Environ. 88 (2009) 479–489, https://doi.org/10.1016/j.apcatb.2008.10.010.
[29] E.R. Wagoner, D.G. Peters, Electrocatalytic Reduction of 1,1,2-Trichloro-1,2,2-trifluoroethane (CFC-113) at Silver Cathodes in Organic and Organic-Aqueous Solvents, J. Electrochem. Soc. 160 (2013) G135–G141, https://doi.org/10.1149/2.018310jes.
[30] G. Fiori, S. Rondinini, G. Sello, A. Vertova, M. Cirja, L. Conti, Electroreduction of volatile organic halides on activated silver cathodes, J. Appl. Electrochem. 35 (2005) 363–368, https://doi.org/10.1007/s10800-005-0798-5.
[31] Y.J. Kim, S.M. Kim, C. Yu, Y. Yoo, E.J. Cho, J.W. Yang, S.W. Kim, Chemoselective Hydrodehalogenation of Organic Halides Utilizing Two-Dimensional Anionic Electrons of Inorganic Electride [Ca2N]+·e−, Langmuir 33 (2017) 954–958, https://doi.org/10.1021/acs.langmuir.6b04152.
[32] M.L. Hitchman, R.A. Spackman, N.C. Ross, C. Agra, Disposal Methods for Chlorinated Aromatic Waste, Chem. Soc. Rev. 24 (1995) 423–430, https://doi.org/10.1039/cs9952400423.
[33] B. Huang, A.A. Isse, C. Durante, C. Wei, A. Gennaro, Electrocatalytic properties of transition metals toward reductive dechlorination of polychloroethanes, Electrochim. Acta 70 (2012) 50–61, https://doi.org/10.1016/j.electacta.2012.03.009.
[34] C. Durante, B. Huang, A.A. Isse, A. Gennaro, Electrocatalytic dechlorination of volatile organic compounds at copper cathode. Part II: Polychloroethanes, Appl. Catal. B Environ. 126 (2012) 355–362, https://doi.org/10.1016/j.apcatb.2012.07.003.
[35] A.A. Isse, S. Gottardello, C. Maccato, A. Gennaro, Silver nanoparticles deposited on glassy carbon. Electrocatalytic activity for reduction of benzyl chloride, Electrochem. Commun. 8 (2006) 1707–1712, https://doi.org/10.1016/j.elecom.2006.08.001.
[36] C. Durante, V. Perazzolo, L. Perini, M. Favaro, G. Granozzi, A. Gennaro, Electrochemical activation of carbon–halogen bonds: Electrocatalysis at silver/copper nanoparticles, Appl. Catal. B Environ. 158–159 (2014) 286–295, https://doi.org/10.1016/j.apcatb.2014.04.023.
[37] C. Durante, V. Perazzolo, A.A. Isse, M. Favaro, G. Granozzi, A. Gennaro, Electrochemical Activation of Carbon-Halogen Bonds: Electrocatalysis at Palladium-Copper Nanoparticles, ChemElectroChem 1 (2014) 1370–1381, https://doi.org/10.1002/celc.201402032.
[38] L. Perini, C. Durante, M. Favaro, S. Agnoli, G. Granozzi, A. Gennaro, Electrocatalysis at palladium nanoparticles: Effect of the support nitrogen doping on the catalytic activation of carbonhalogen bond, Appl. Catal. B Environ. 144 (2014) 300–307, https://doi.org/10.1016/j.apcatb.2013.07.023.
[39] Y. Lou, J. Fontmorin, A. Amrane, F. Fourcade, F. Geneste, Metallic nanoparticles for electrocatalytic reduction of halogenated organic compounds: A review, Electrochim. Acta 377 (2021), 138039, https://doi.org/10.1016/j.electacta.2021.138039.
[40] Y.H. Xu, H. Zhang, C.P. Chu, C.A. Ma, Dechlorination of chloroacetic acids by electrocatalytic reduction using activated silver electrodes in aqueous solutions of different pH, J. Electroanal. Chem. 664 (2012) 39–45, https://doi.org/10.1016/j.jelechem.2011.10.010.
[41] Y. Xu, X. Ding, H. Ma, Y. Chu, C. Ma, Selective hydrodechlorination of 3,5,6-trichloropicolinic acid at an activated silver cathode: Synthesis of 3,5-dichloropicolinic acid, Electrochim. Acta 151 (2015) 284–288, https://doi.org/10.1016/j.electacta.2014.11.039.
[42] H.-X. Ma, T.-J. Ge, Q.-Q. Cai, Y.-H. Xu, C.-A. Ma, Catalytic Effect of Silver Cathodes on 3,4,5,6-Tetrachloropicolinic Acid Dechlorination in Aqueous Solutions, Acta Phys.-Chim. Sin. 32 (2016) 1715–1721, https://doi.org/10.3866/pku.Whxb201604121.
[43] S. Ardizzone, G. Cappelletti, L.M. Doubova, P.R. Mussini, S.M. Passeri, S. Rondinini, The role of surface morphology on the electrocatalytic reduction of organic halides on mono- and polycrystalline silver, Electrochim. Acta 48 (2003) 3789–3796, https://doi.org/10.1016/s0013-4686(03)00512-7.